*Tectonics*

Supporting Information for

# The Limpopo magma-rich transform margin (South Mozambique) – Part 1: Insights from deep-structure seismic imaging

L. Watremez[1], S. Leroy[2], E. d'Acremont[2], V. Roche[2], M. Evain[3], A. Leprêtre[3], F. Verrier[3], D. Aslanian[3], N. Dias[4,5], A. Afilhado[4,5], P. Schnurle[3], R. Castilla[6], F. Despinois[7], M. Moulin[3]

[1] Univ. Lille, CNRS, Univ. Littoral Côte d'Opale, IRD, UMR 8187 – LOG – Laboratoire d'Océanologie et de Géosciences, F-59000 Lille, France
[2] Sorbonne Université, CNRS, Institut des Sciences de la Terre de Paris, UMR 7193, ISTeP, Paris, France
[3] IFREMER, REM/GM/LGS, Centre de Brest, Plouzané, France
[4] Instituto Dom Luis (IDL), Faculdade das Ciências, Universidade de Lisboa, Campo Grande, 1749-016 Lisboa, Portugal
[5] Instituto Superior de Engenharia de Lisboa, Instituto Politécnico de Lisboa, 1959-007 Lisboa, Portugal
[6] Géo-Energie, Zürich, Switzerland
[7] Total Exploration et Production, Pau, France
Corresponding author: Louise Watremez (Louise.Watremez@univ-lille.fr)

## Contents of this file

## Supplementary Material 1: Tomography models

Tomo2D (Korenaga et al., 2000) allowed us to model the crustal, Moho and mantle phases in the offshore part of both models, using the layered tomography modelling of Sallarès et al. (2011). We used the sediment velocities and top basement interface from the Rayinvr modelling, together with typical crustal velocities below this reflector, as the input model for the first computation step. The first step produced a model using all the first arrival times (refractions) down the lower crust and the Moho reflections. The result of this first model was used as input for the second step in which we calculated the upper-most mantle velocities, as the Moho depths were updated. Figures S1.1 and S1.2 show the final tomography results and comparisons with Rayinvr velocities.

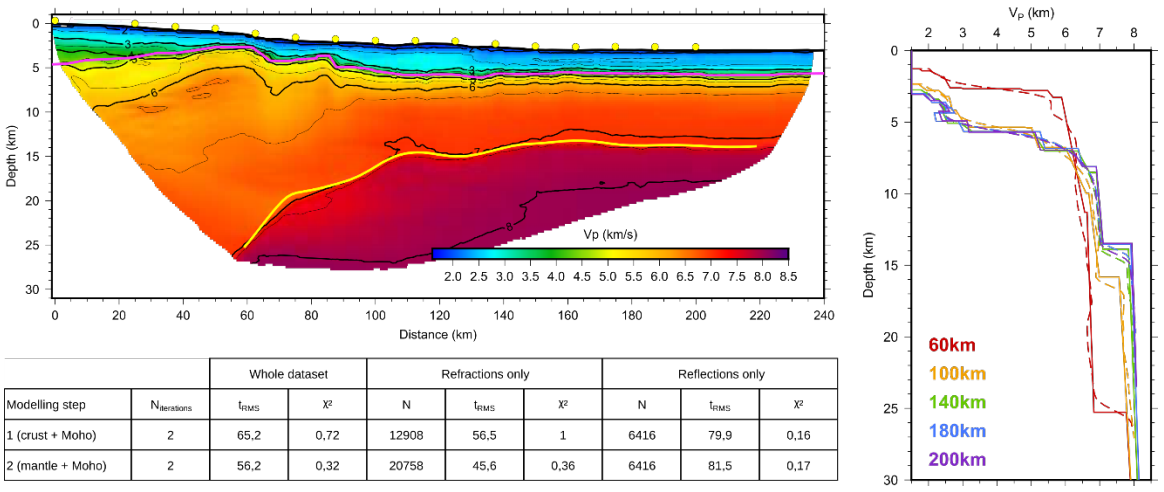


| | | Whole dataset | | Refractions only | | | Reflections only | | |
|---|---|---|---|---|---|---|---|---|---|
| Modelling step | $N_{iterations}$ | $t_{RMS}$ | $\chi^2$ | N | $t_{RMS}$ | $\chi^2$ | N | $t_{RMS}$ | $\chi^2$ |
| 1 (crust + Moho) | 2 | 65,2 | 0,72 | 12908 | 56,5 | 1 | 6416 | 79,9 | 0,16 |
| 2 (mantle + Moho) | 2 | 56,2 | 0,32 | 20758 | 45,6 | 0,36 | 6416 | 81,5 | 0,17 |

**Figure S1.1.** Results of the tomography layered modelling along MZ4. Top-left panel: final tomo2D velocity model. Bottom-left panel: modelling statistics for the two modelling steps. Right panel: comparison of Tomo2D vertical velocity profiles (dashed lines) with the coincident Rayinvr profiles (continuous lines) at different model locations (color code to the left).

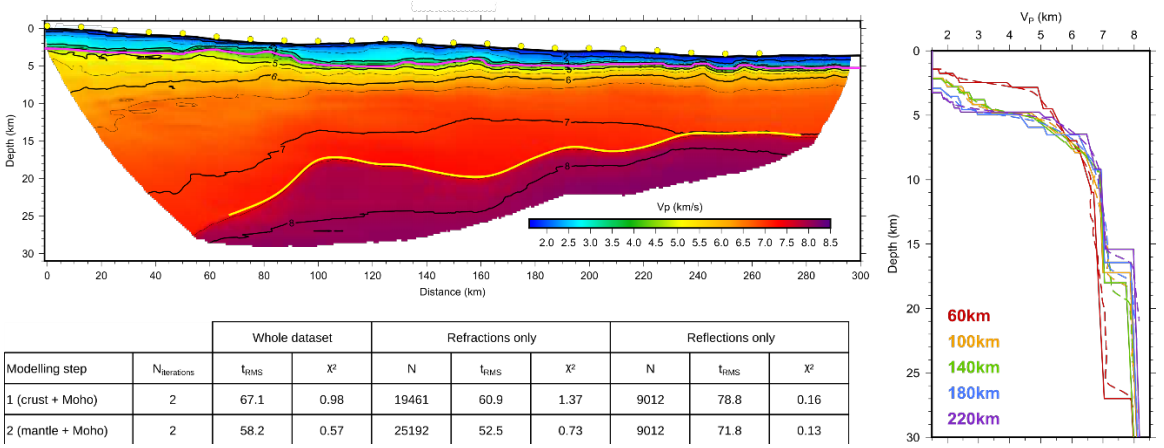


| | | Whole dataset | | Refractions only | | | Reflections only | | |
|---|---|---|---|---|---|---|---|---|---|
| Modelling step | $N_{iterations}$ | $t_{RMS}$ | $\chi^2$ | N | $t_{RMS}$ | $\chi^2$ | N | $t_{RMS}$ | $\chi^2$ |
| 1 (crust + Moho) | 2 | 67.1 | 0.98 | 19461 | 60.9 | 1.37 | 9012 | 78.8 | 0.16 |
| 2 (mantle + Moho) | 2 | 58.2 | 0.57 | 25192 | 52.5 | 0.73 | 9012 | 71.8 | 0.13 |

**Figure S1.2.** Results of the tomography layered modelling along MZ5. Top-left panel: final tomo2D velocity model. Bottom-left panel: modelling statistics for the two modelling steps. Right panel: comparison of Tomo2D vertical velocity profiles (dashed lines) with the coincident Rayinvr profiles (continuous lines) at different model locations (color code to the left).

Sallarès, V., Gailler, A., Gutscher, M. A., Graindorge, D., Bartolomé, R., Gracia, E., Dìaz, J., Dañobeitia, J. J., & Zitellini, N., 2011. Seismic evidence for the presence of Jurassic oceanic crust in the central Gulf of Cadiz (SW Iberian margin). Earth and Planetary Science Letters, 311(1-2), 112-123, doi:10.1016/j.epsl.2011.09.003.

Korenaga, J., Holbrook, W. S., Kent, G. M., Kelemen, P. B., Detrick, R. S., Larsen, H. C., Hopper, J. R., & Dahl-Jensen, T., 2000. Crustal structure of the southeast Greenland margin from joint refraction and reflection seismic tomography. Journal of Geophysical Research: Solid Earth, 105(B9), 21591-21614, doi:10.1029/2000JB900188.

## Supplementary Material 2: Picking uncertainties

The uncertainties for each pick are computed using the signal-to-noise ratio (S/N) along the trace, using a window of 250 ms before and after the pick. We followed a slightly modified version of the parametrization from Zelt & Forsyth (1994). Our parametrization is shown in the table below. High S/N values give the smallest uncertainties (25 ms) while the picks on noisy data (low S/N) give the highest uncertainties (250 ms). The S/N ratio being low for the reflection phases at short offsets (beneath the direct arrival), we decided to reduce the uncertainties for offsets < 30 km to allow for proper fitting of the sediment reflections without getting very low $\chi^2$ values when we know where the reflections from the MCS data are. If the source-receiver distance (x) is greater than 30 km, the final uncertainty ($unc_f$) is equal to the base uncertainty ($unc_{base}$). Else, $unc_f = unc_{base} \times \left(0.4 + \frac{|x| \times 0.6}{30\ 10^3}\right)$, with x, in meters.

| S/N | Base uncertainty (ms) |
|---|---|
| > 10 | 25 |
| 4-10 | 35 |
| 2-4 | 50 |
| 1.75-2 | 75 |
| 1.5-1.75 | 100 |
| 1.1-1.5 | 125 |
| < 1.1 | 250 |

**Table S2.1.** Uncertainty parametrization from the signal to noise ratio (comparison of the RMS amplitudes 250 ms before and after the pick).

Zelt, C. A. & Forsyth, D. A., 1994. Modeling wide-angle seismic data for crustal structure: Southeastern Grenville Province. Journal of Geophysical Research: Solid Earth, 99(B6), 11687-11704, doi:10.1029/93JB02764.

## Supplementary Material 3: Fits

The figures S3.1. and S3.2. present the fits for all the instruments. The on land seismometers (LSS) are shown with a reduction velocity of 7 km/s while the OBS are shown with three different reduction velocities (3.5, 5 and 7 km/s). The colored bars represent the picked travel-times with corresponding uncertainty and the black dots represent the computed travel-times, from raytracing in the velocity models. The line number and instrument identifications are shown above each plot. The color codes are the same as in Figure 3. The velocity reduction is shown on the left of each plot.

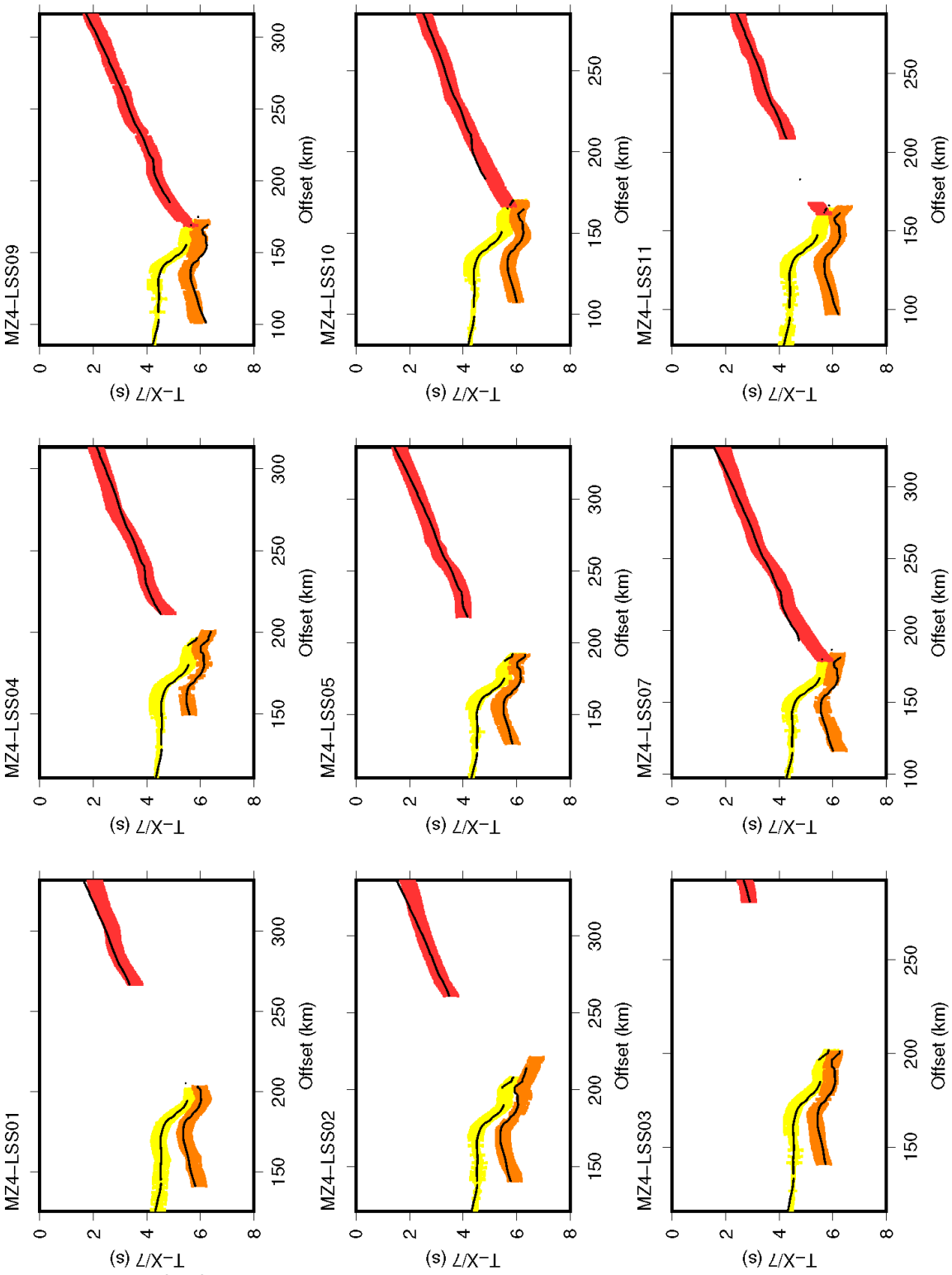


**Figure S3.1.** All fits for MZ4

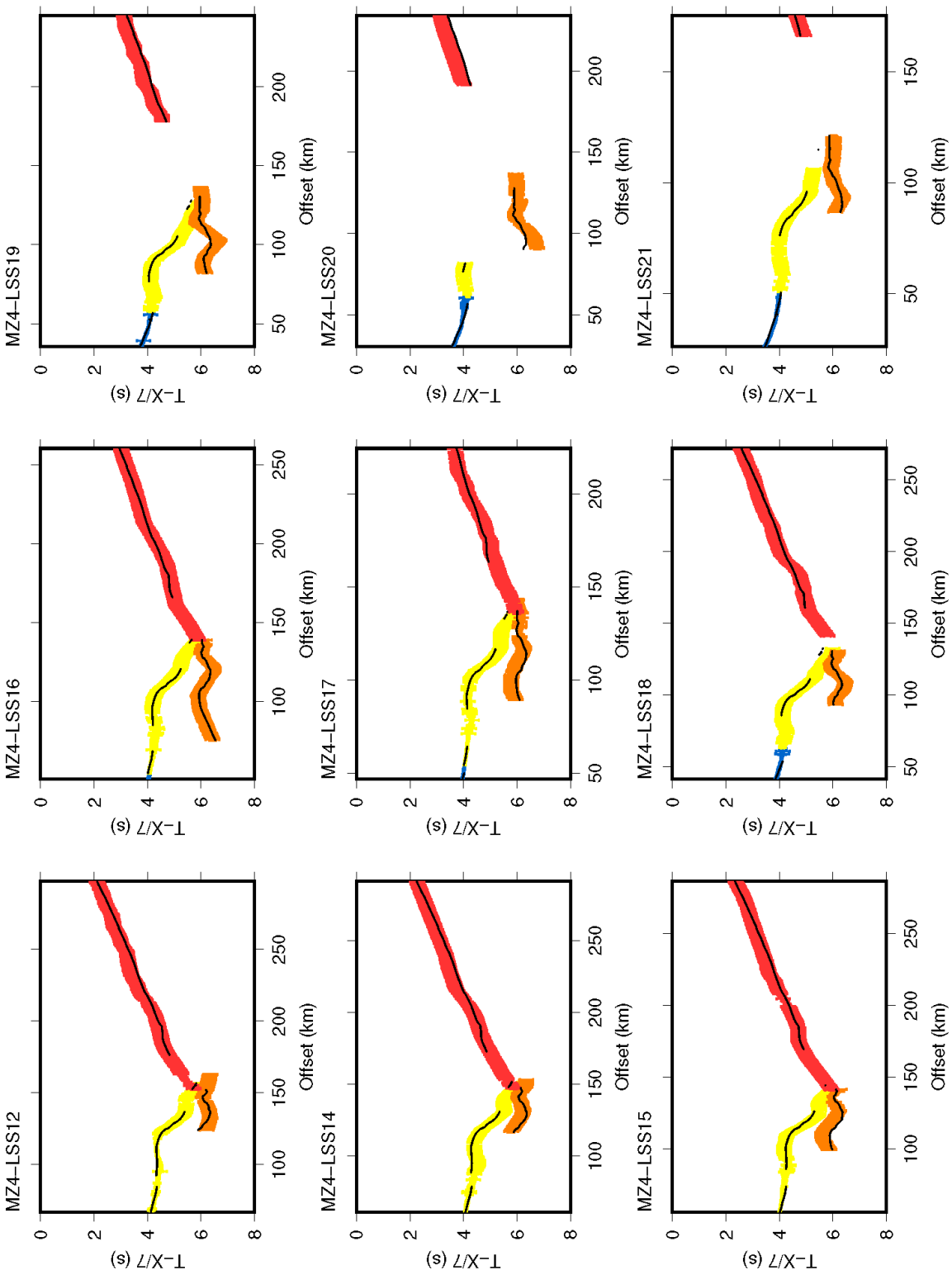


**Figure S3.1.** All fits for MZ4 (continued)

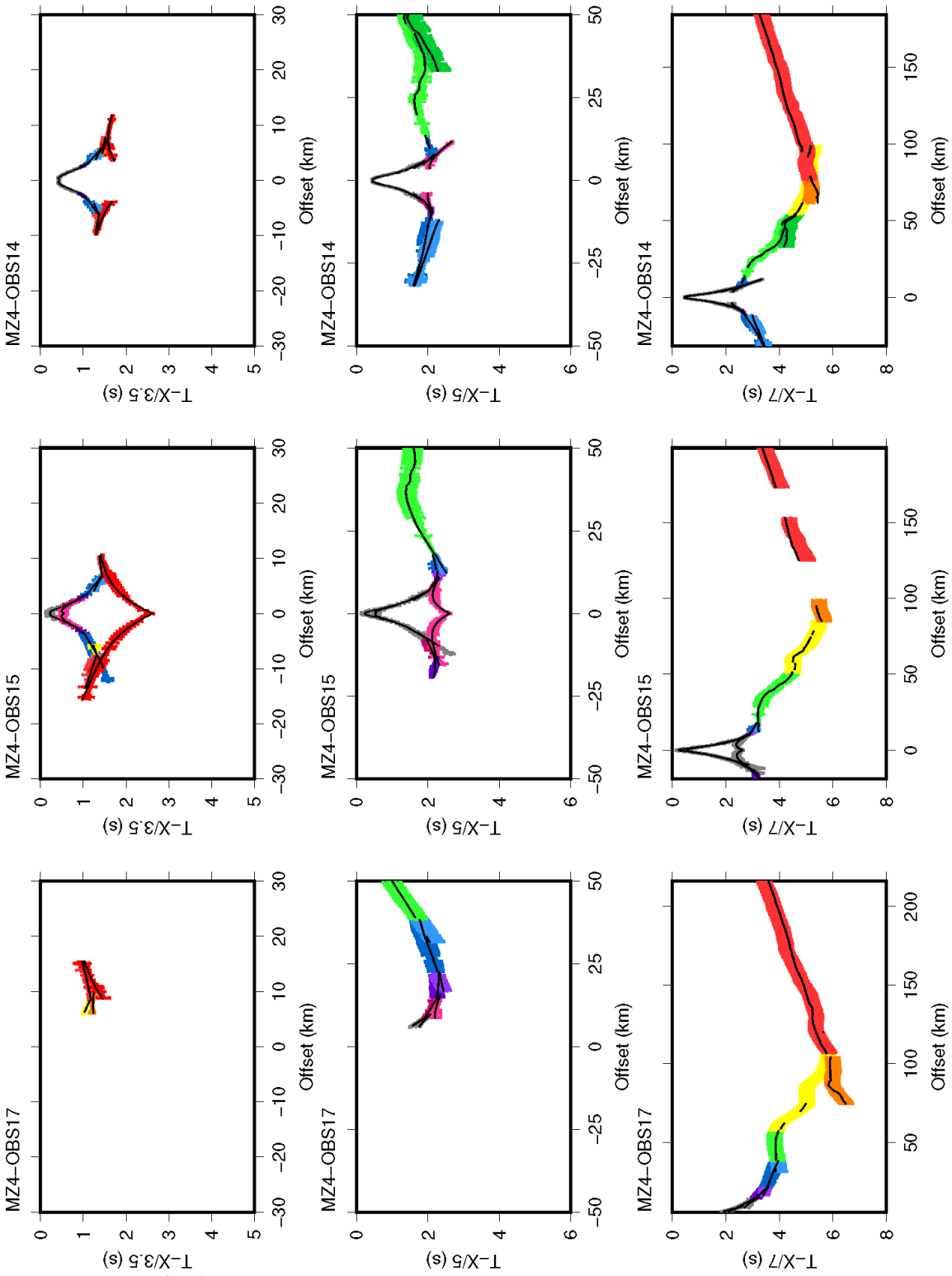


**Figure S3.1.** All fits for MZ4 (continued)

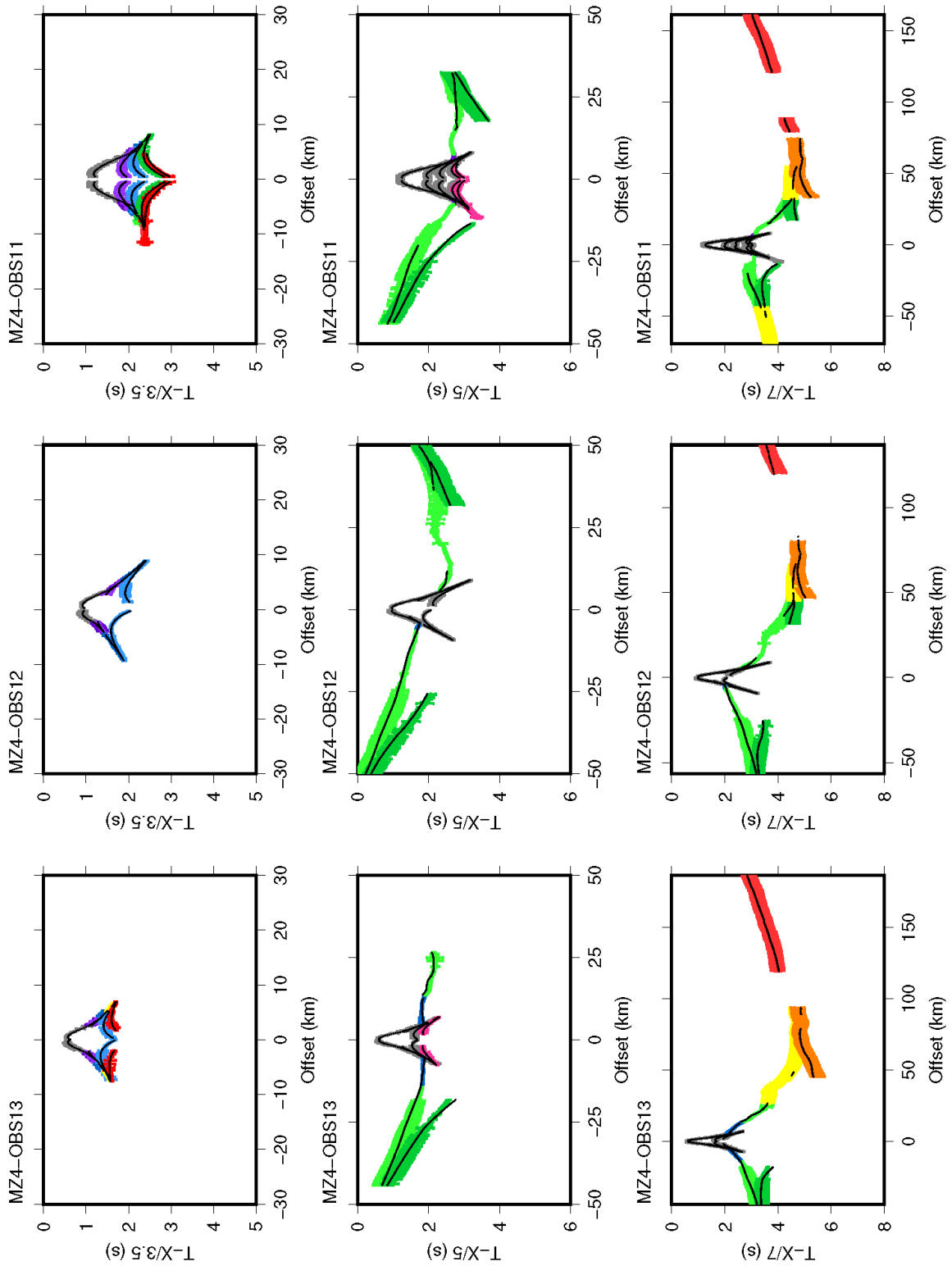


**Figure S3.1.** All fits for MZ4 (continued)

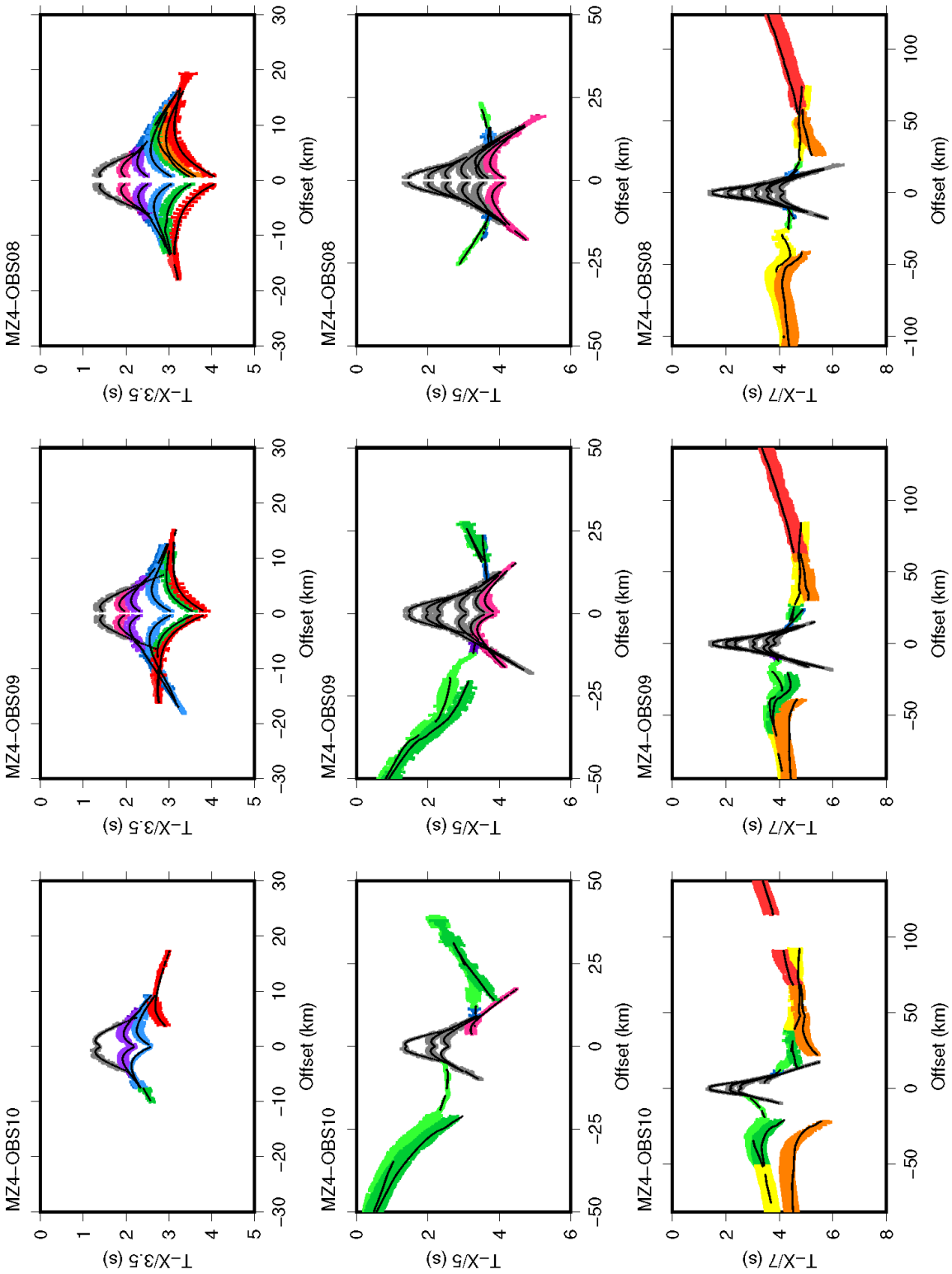


**Figure S3.1.** All fits for MZ4 (continued)

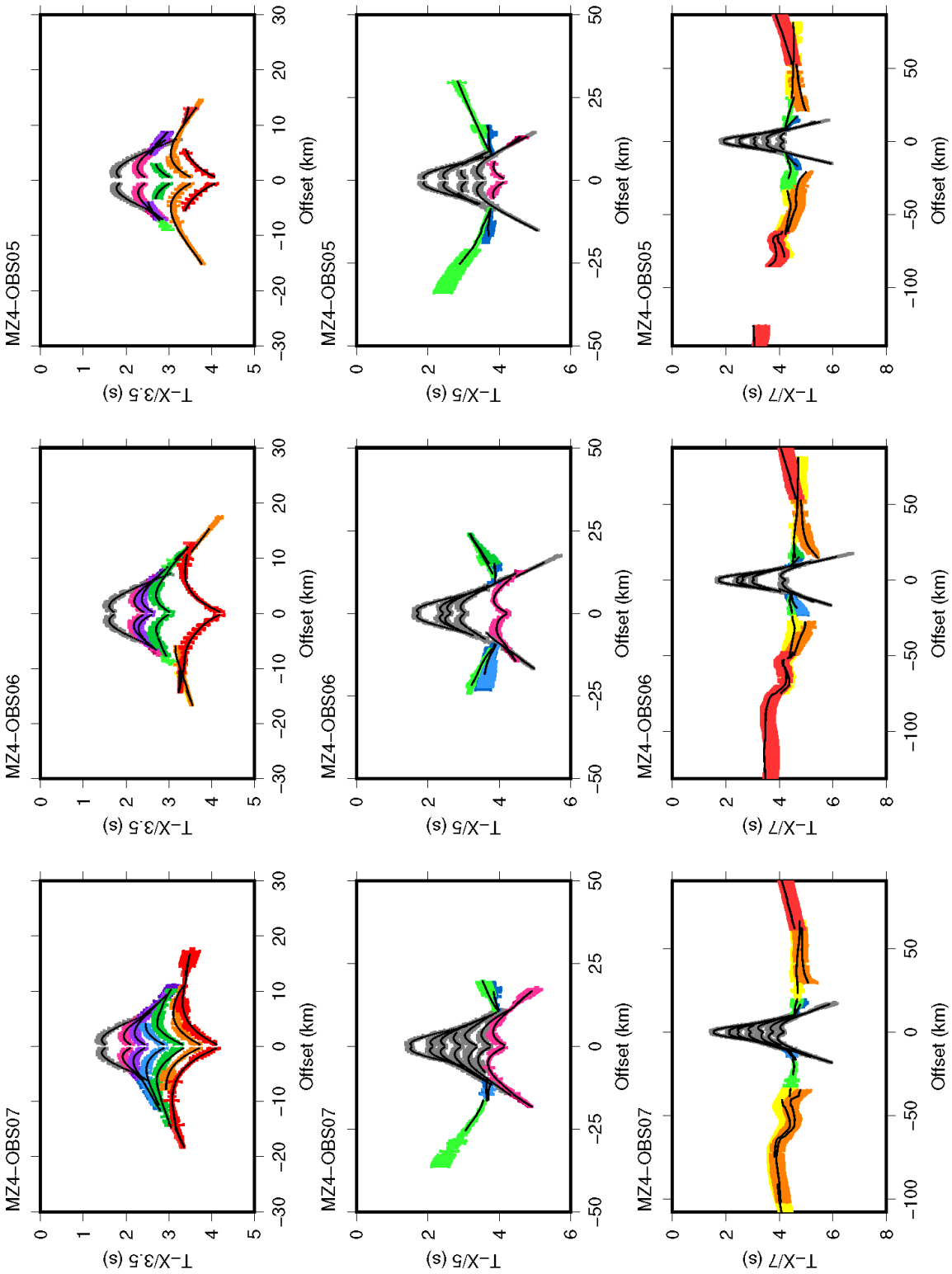


**Figure S3.1.** All fits for MZ4 (continued)

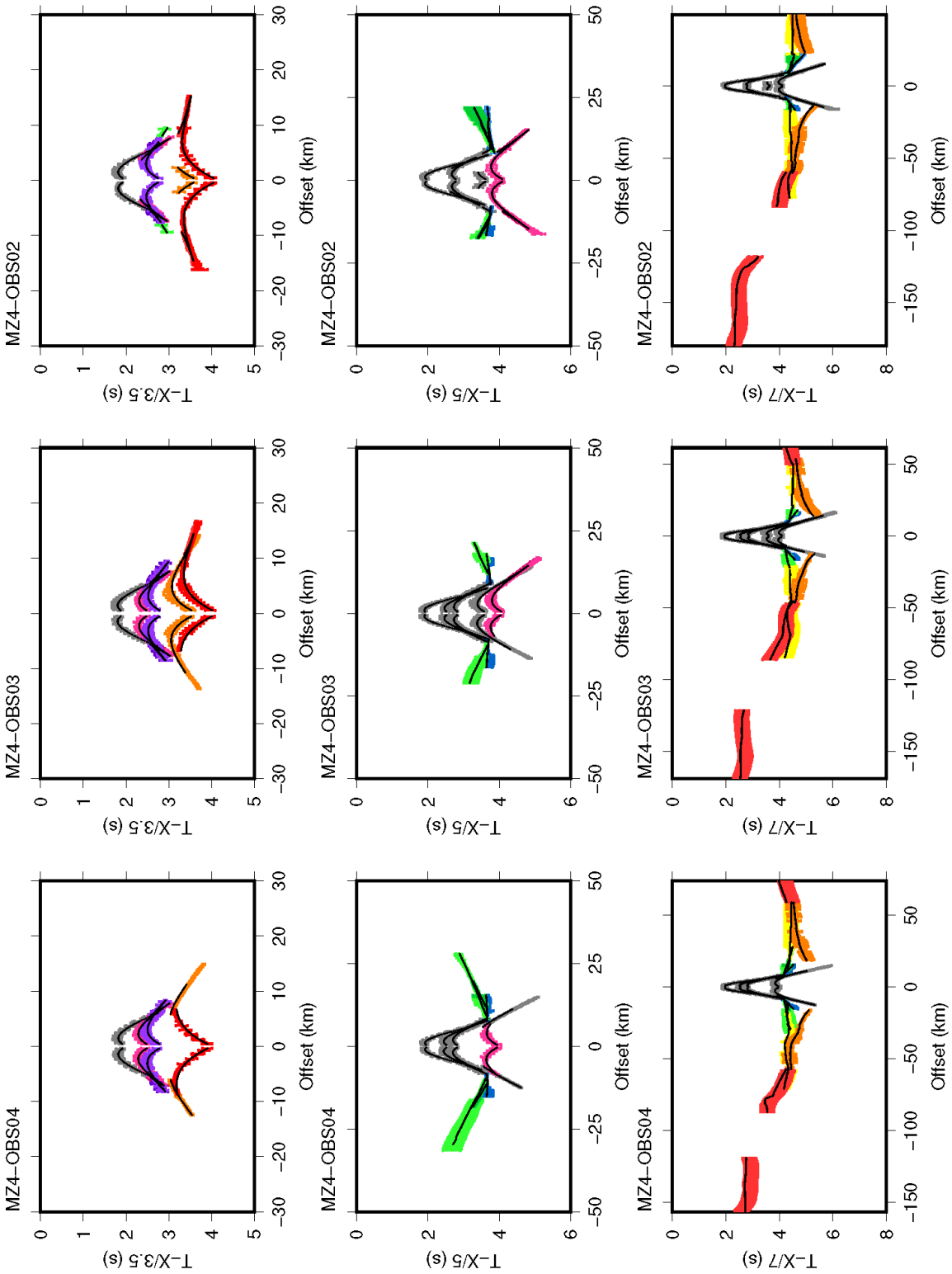


**Figure S3.1.** All fits for MZ4 (continued)

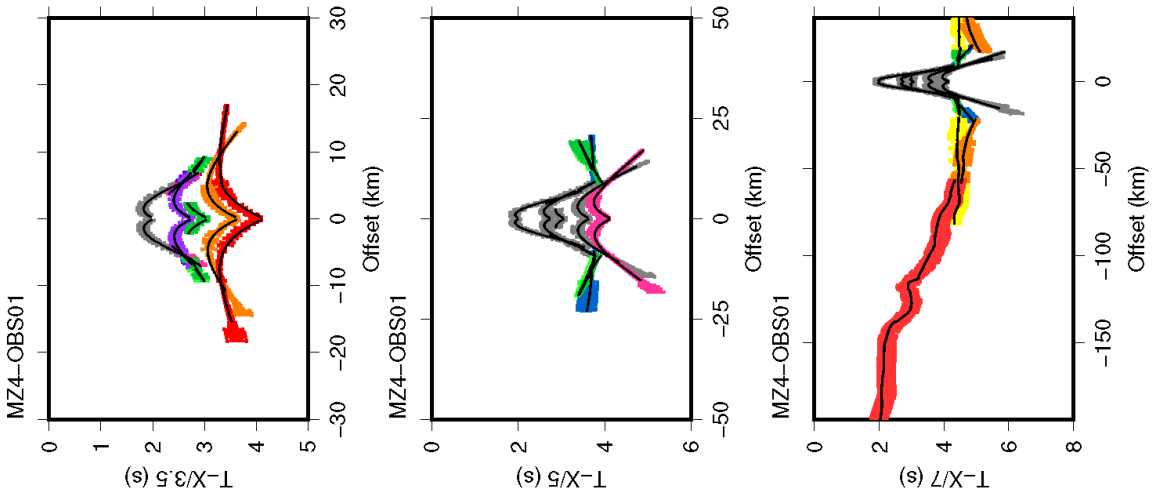


**Figure S3.1.** All fits for MZ4 (continued)

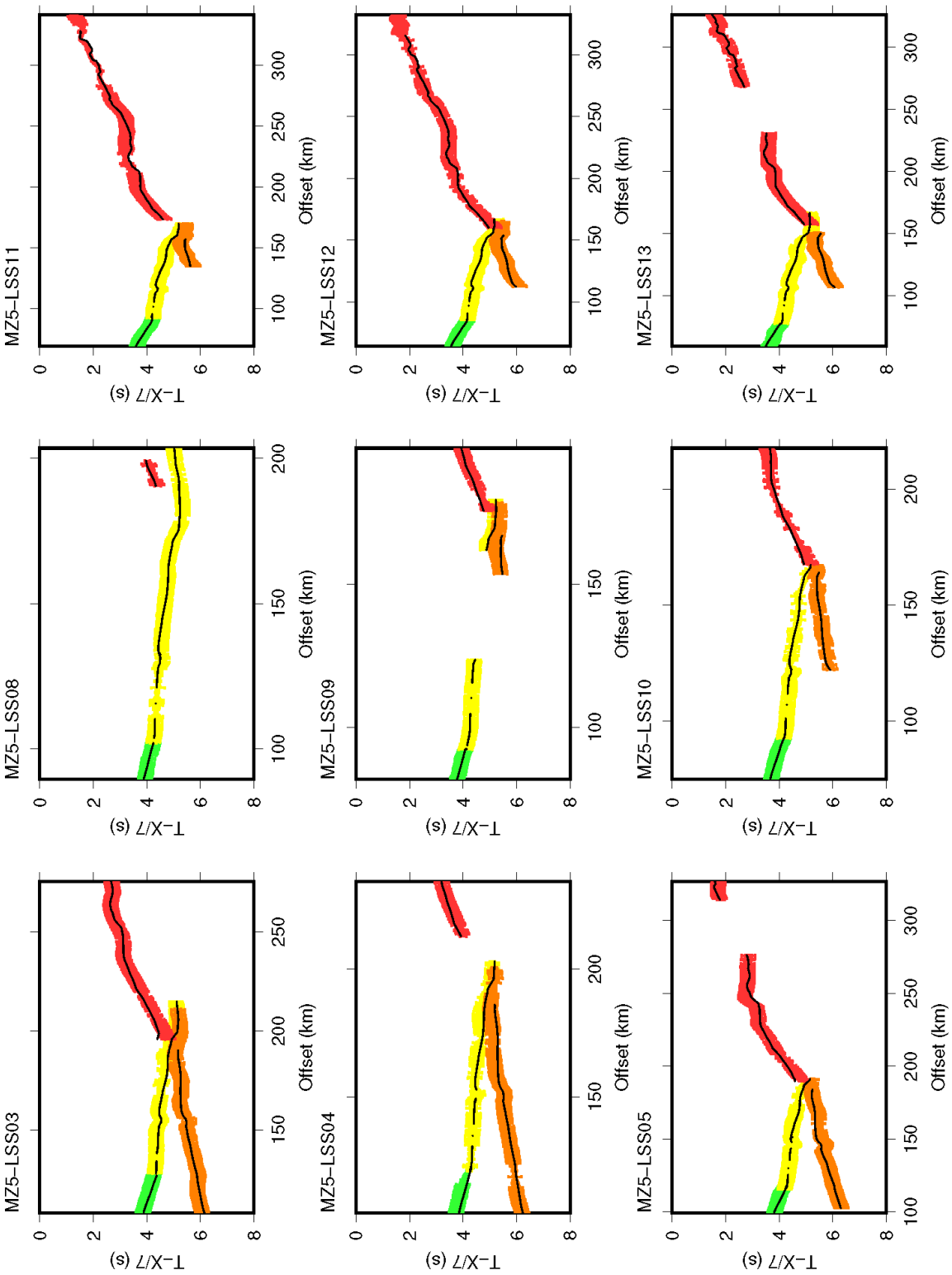


**Figure S3.2.** All fits for MZ5

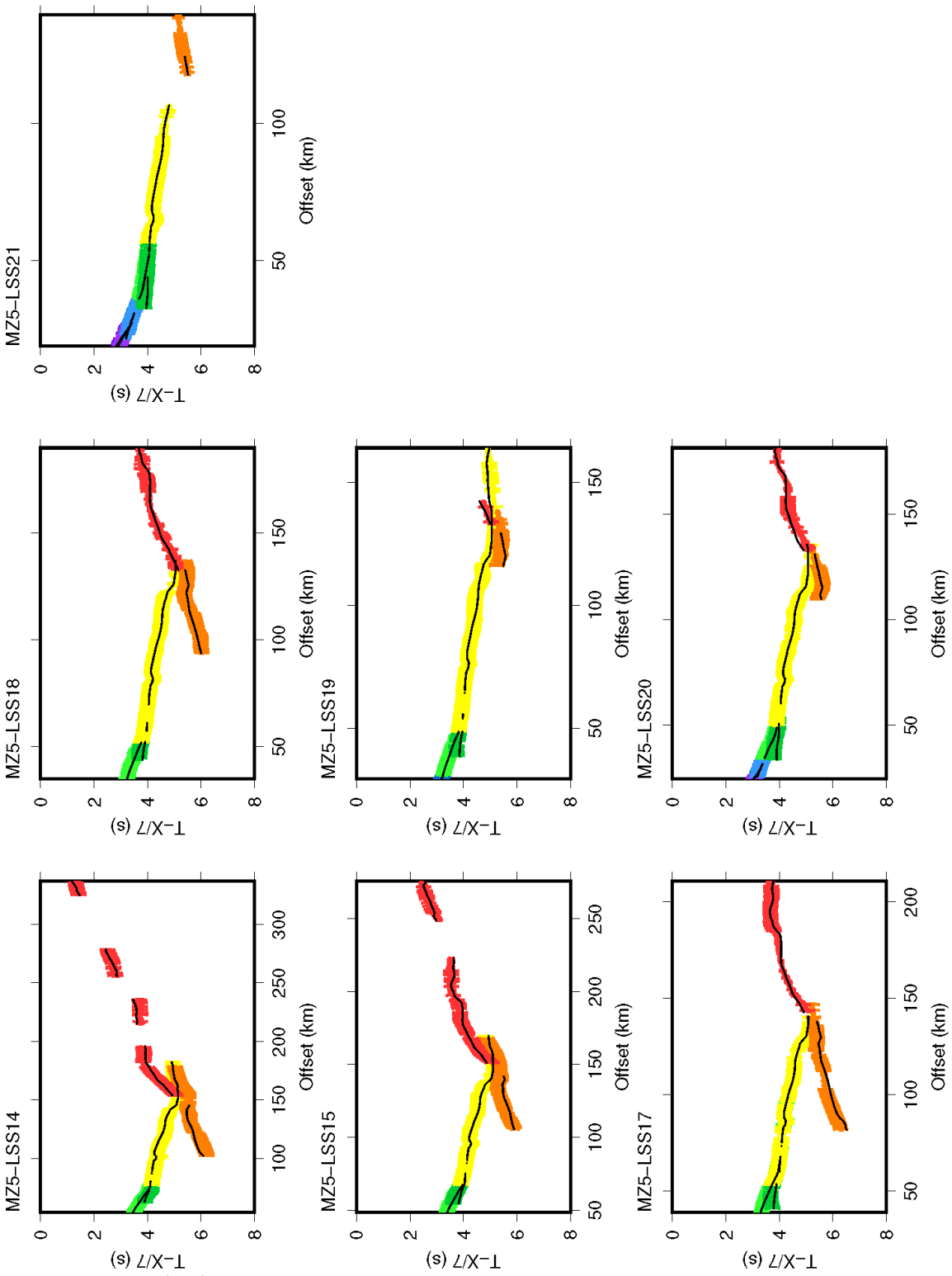


**Figure S3.2.** All fits for MZ5 (continued)

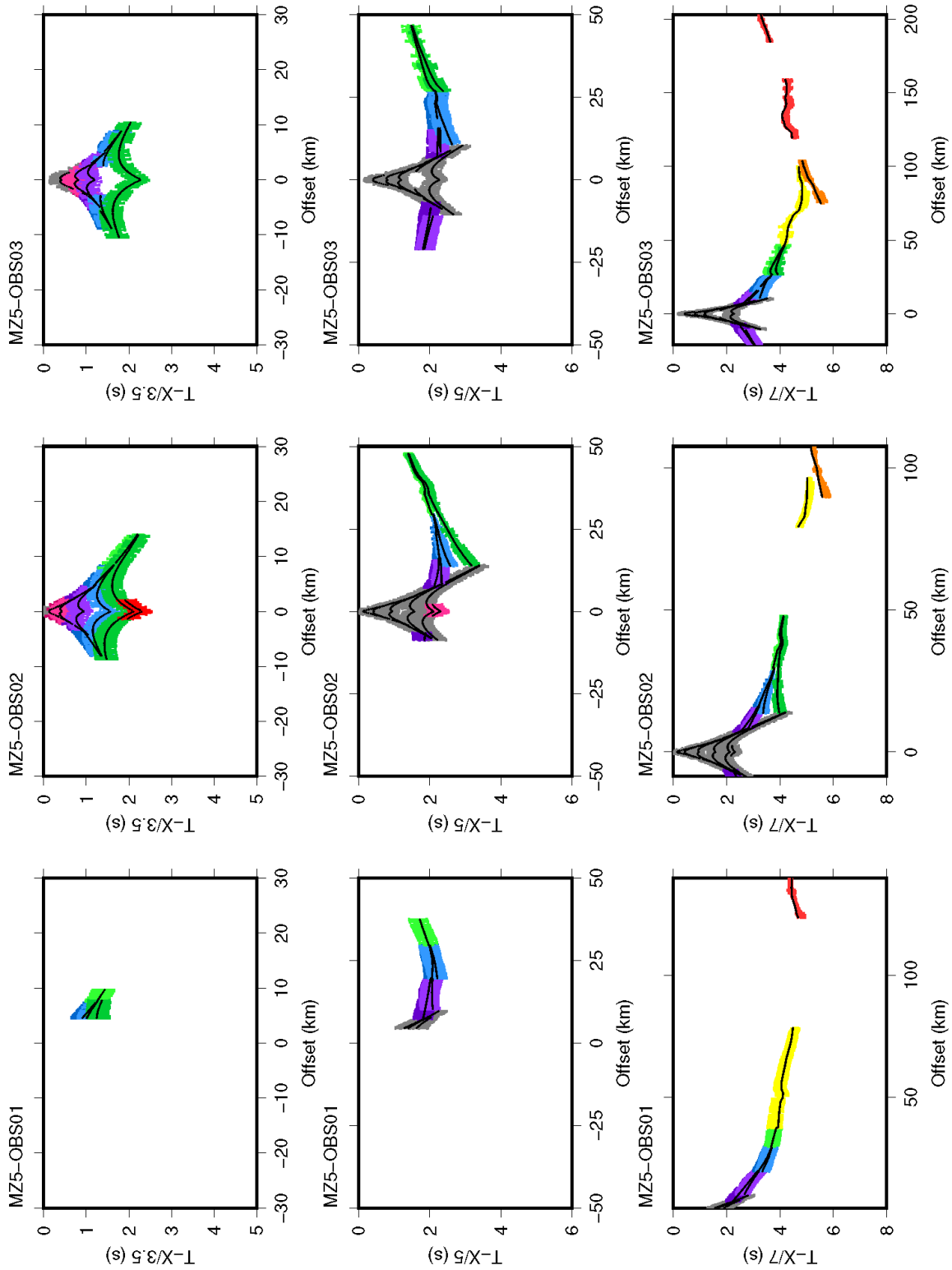


**Figure S3.2.** All fits for MZ5 (continued)

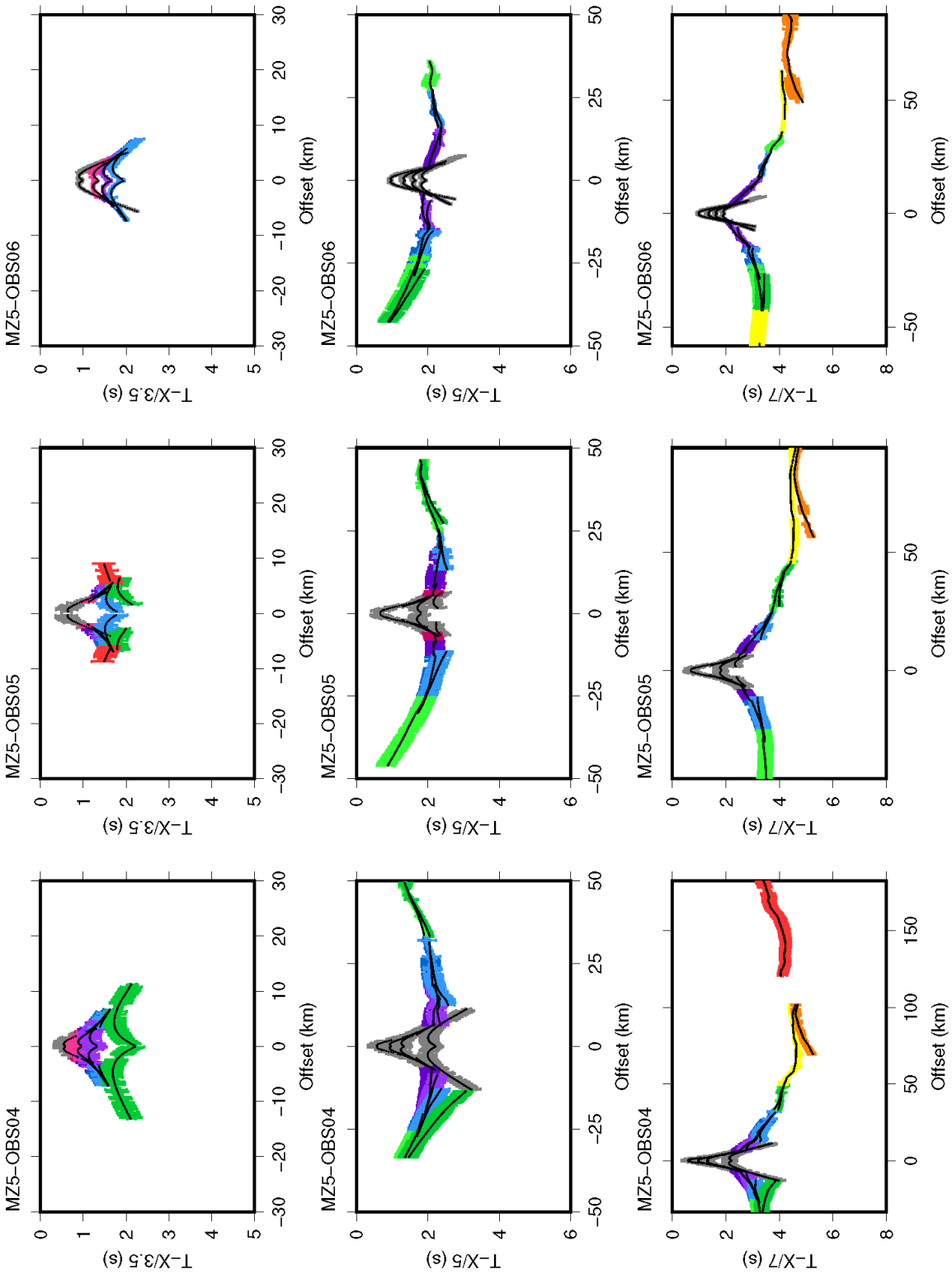


**Figure S3.2.** All fits for MZ5 (continued)

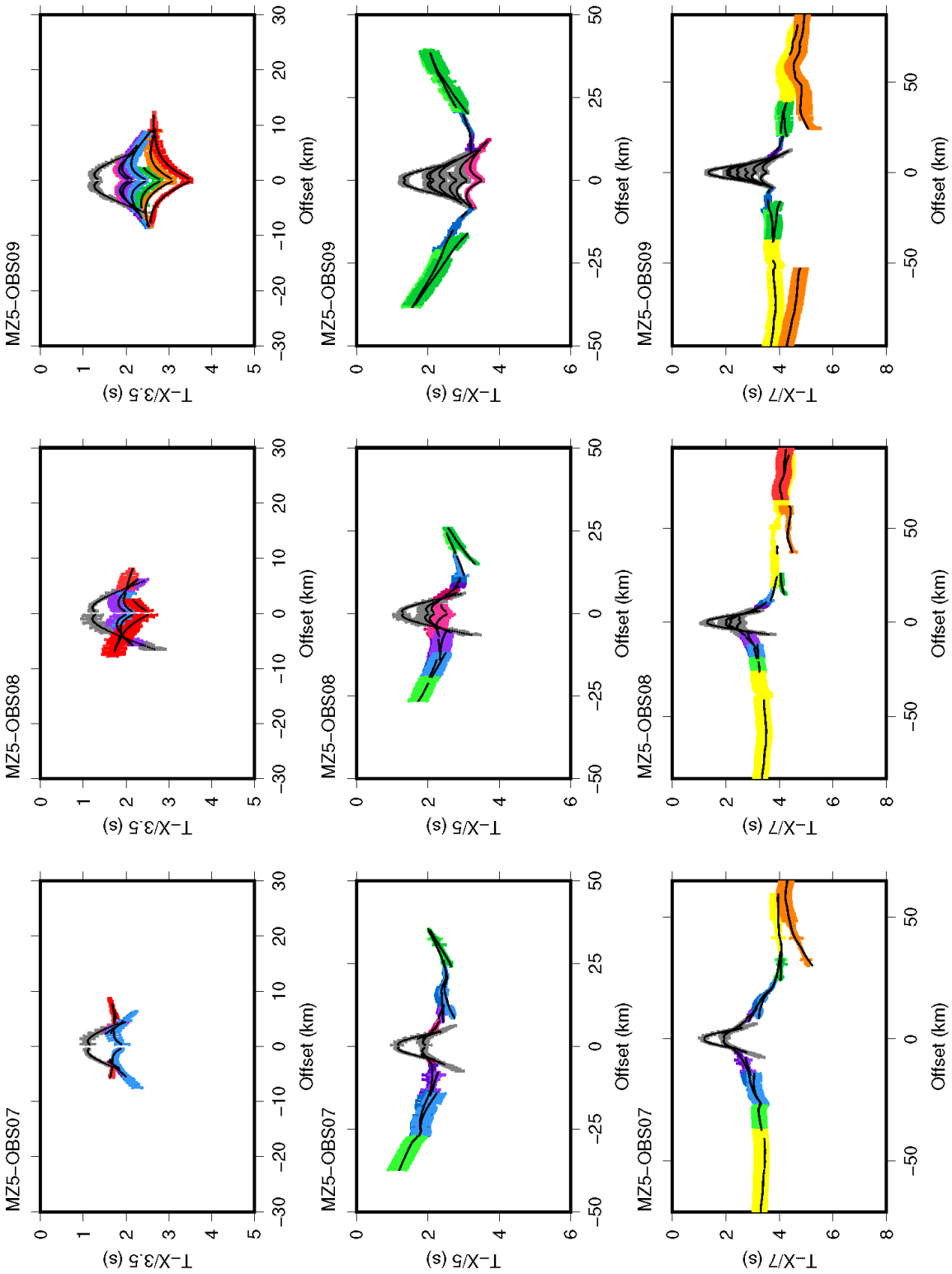


**Figure S3.2.** All fits for MZ5 (continued)

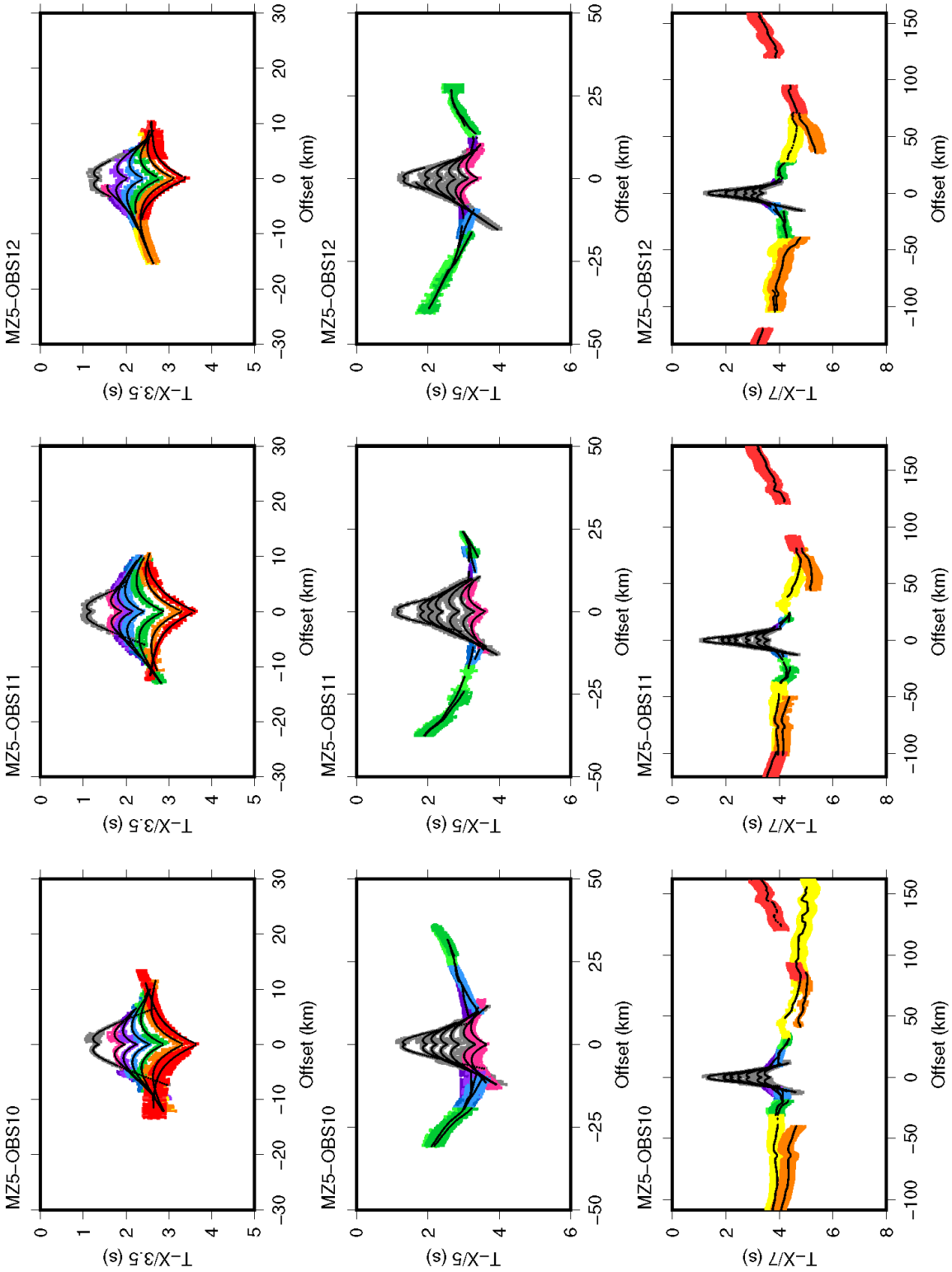


**Figure S3.2.** All fits for MZ5 (continued)

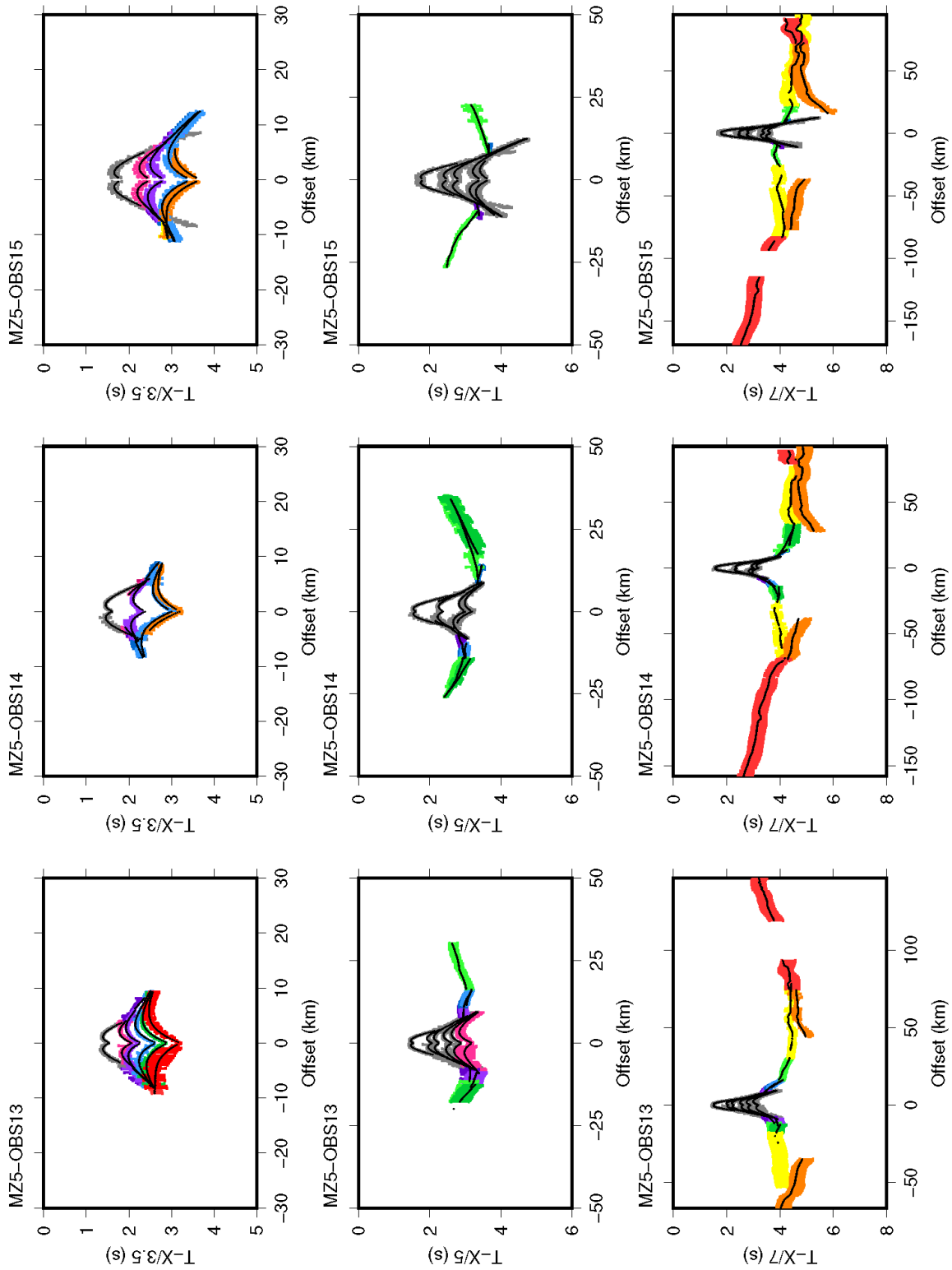


**Figure S3.2.** All fits for MZ5 (continued)

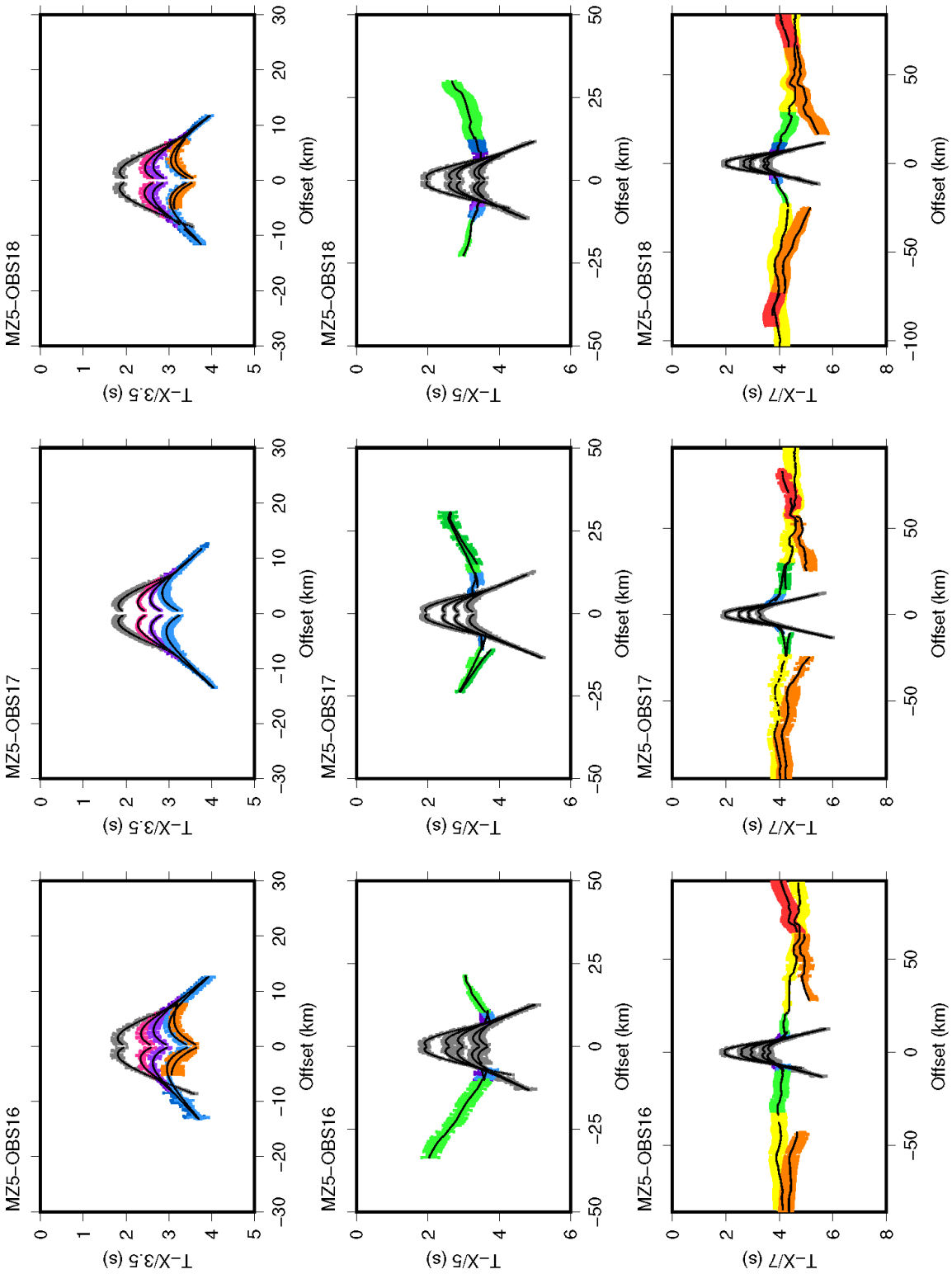


**Figure S3.2.** All fits for MZ5 (continued)

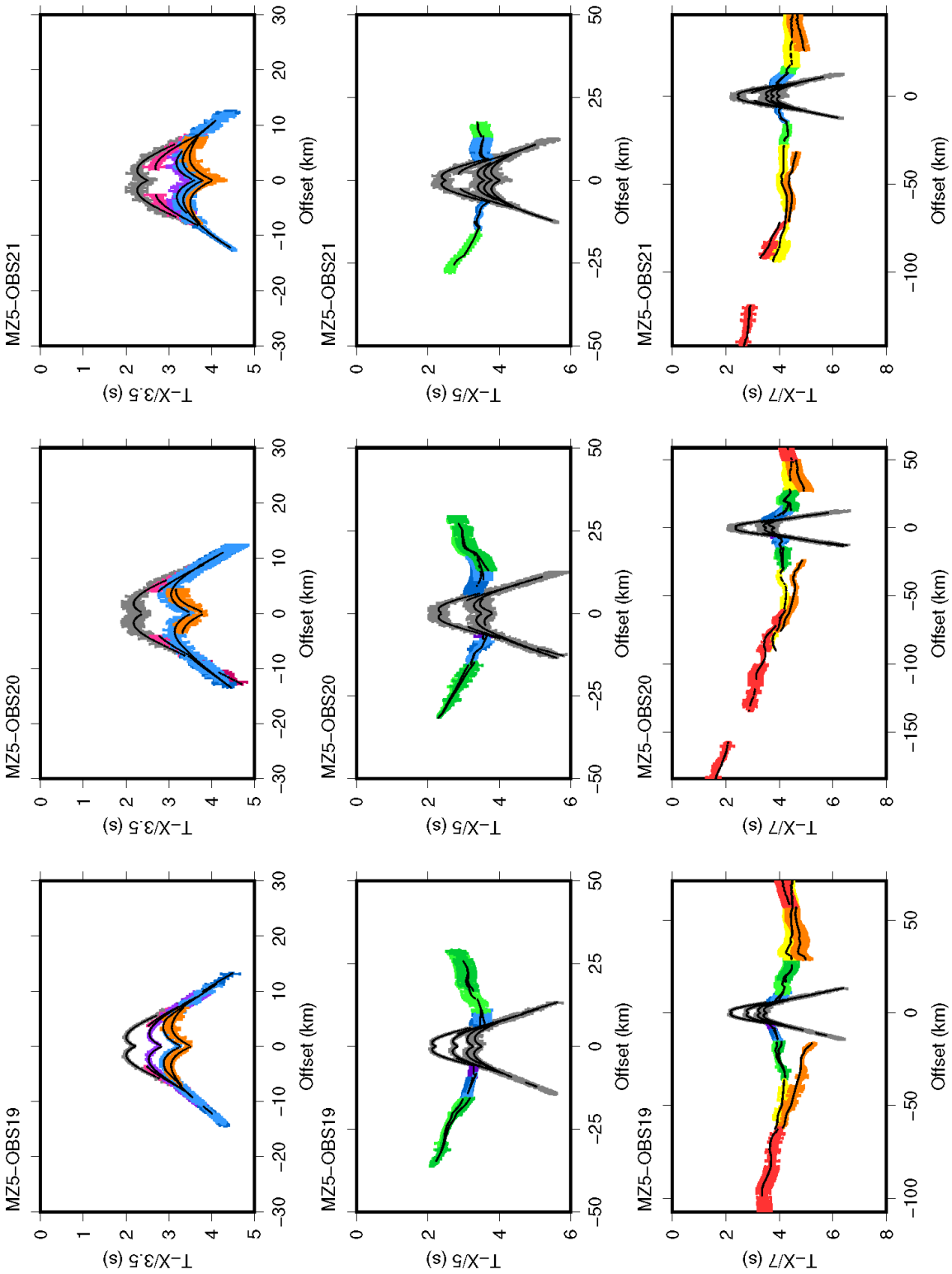


**Figure S3.2.** All fits for MZ5 (continued)

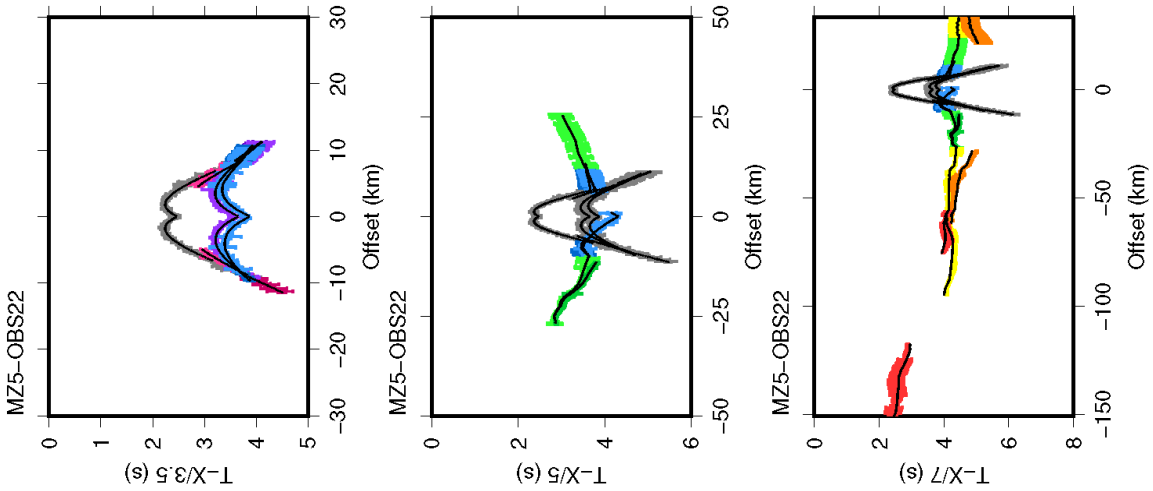


**Figure S3.2.** All fits for MZ5 (continued)

## Supplementary Material 4: Velocity anomaly diagrams

The velocity anomaly diagrams were produced using a systematic modelling of a variety of velocity and/or depth perturbations. We tested perturbations of (1) the lower crustal velocities together with Moho depths and (2) the uppermost mantle velocities, with Moho depths. Thus, two plots for each profile were obtained (Figures S4.1 and S4.2), showing the variations of the root-mean-squared residual traveltimes with the model perturbations. The $t_{RMS}$ values were computed using only the seismic phases that are affected by the anomaly.

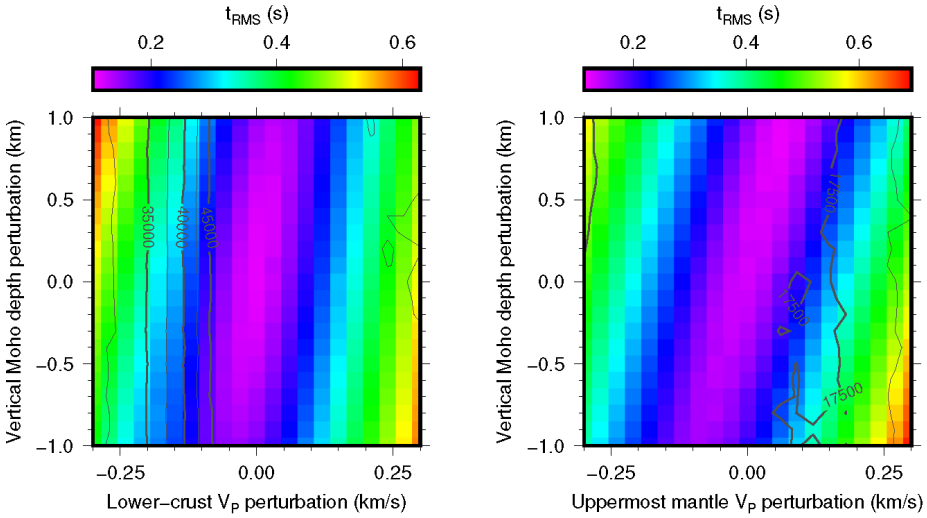


**Figure S4.1.** Velocity anomaly diagrams for the lower crustal and uppermost mantle velocities with the Moho depth for MZ4. The center of the plot corresponds to the final model.

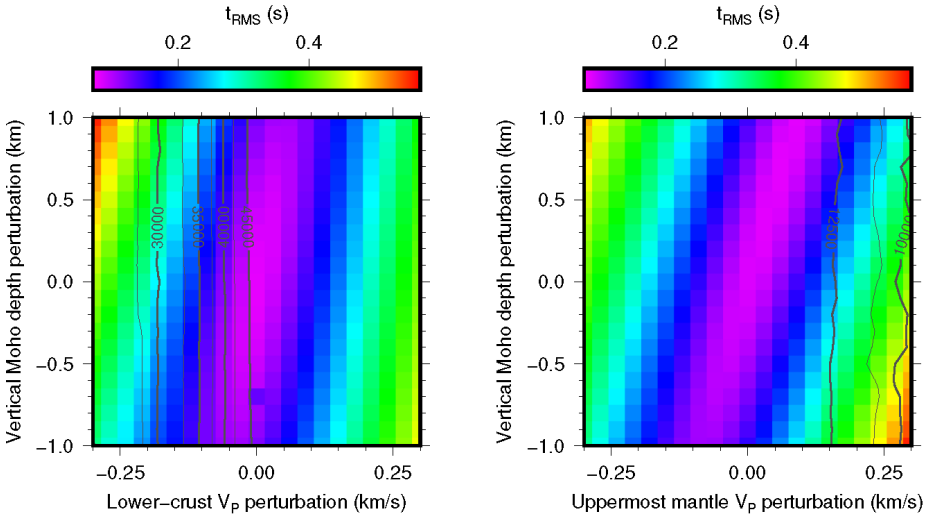


**Figure S4.2.** Velocity anomaly diagrams for the lower crustal and uppermost mantle velocities with the Moho depth for MZ4. The center of the plot corresponds to the final model.

## Supplementary Material 5: Location of tested nodes in VMonteCarlo

VMonteCarlo parameter locations (white hexagons) along MZ4 and MZ5 (Figures S5.1 and S5.2).

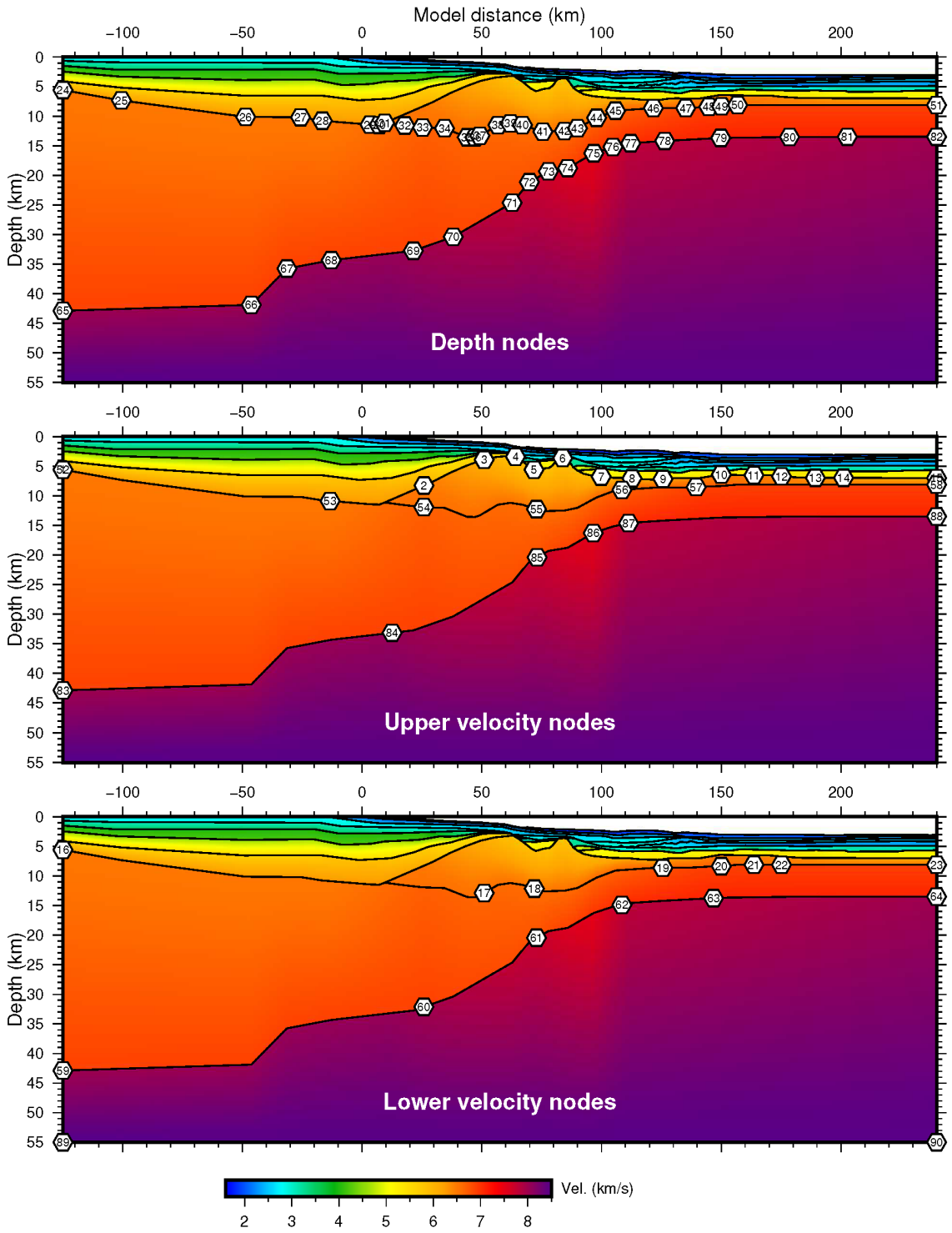


**Figure S5.1.** VMonteCarlo parameter locations along MZ4. The colorscale corresponds to the P-wave velocities in the final model. The top panels correspond to the location of interface depth nodes. Node numbers correspond to the parameter numbers in Table 3.

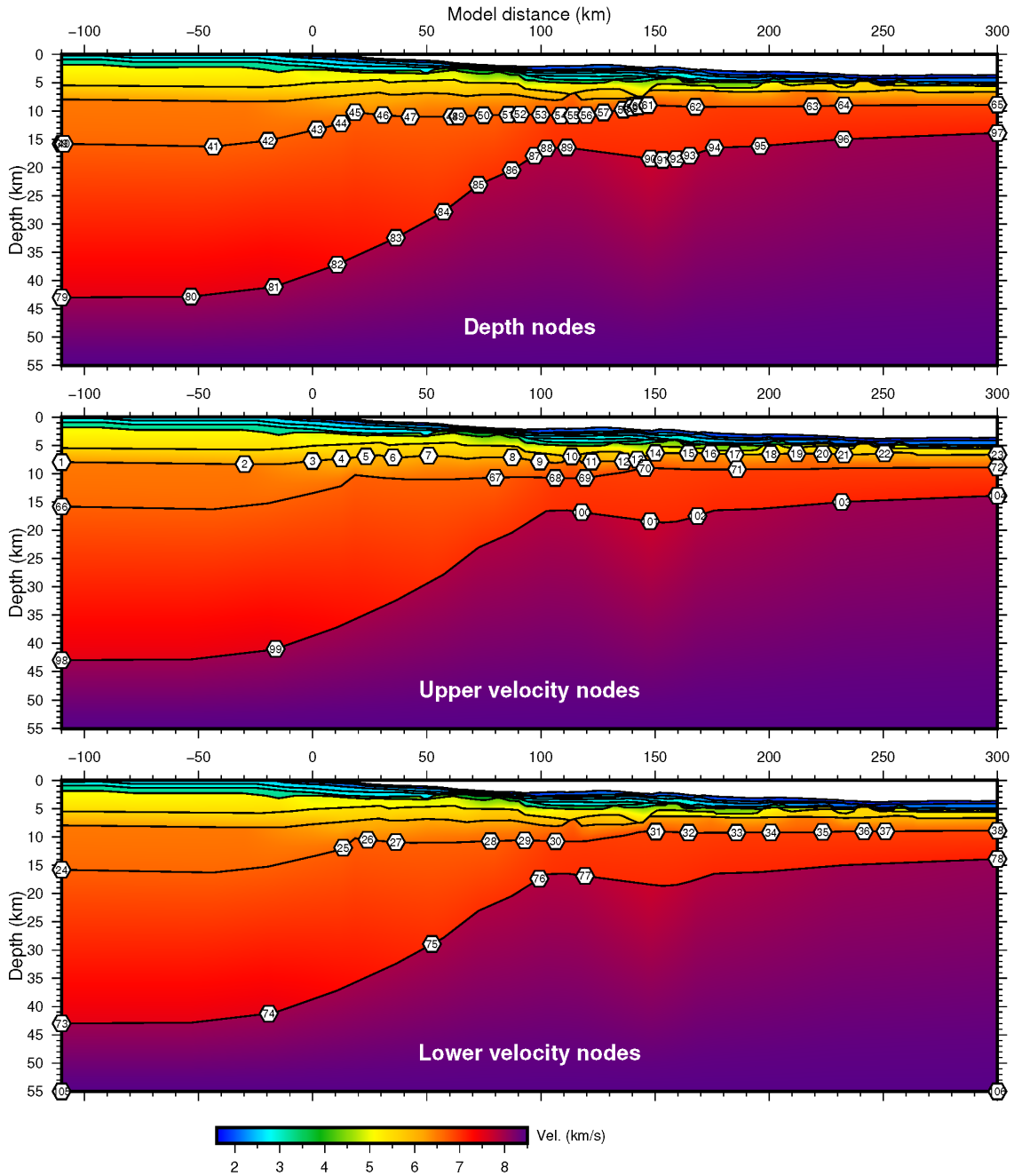


**Figure S5.2.** VMonteCarlo parameter locations along MZ4. The colorscale corresponds to the P-wave velocities in the final model. The top panels correspond to the location of interface depth nodes. Node numbers correspond to the parameter numbers in Table 3.